Received: 23 November 2023 | Revised: 5 March 2024 | Accepted: 29 March 2024

DOI: 10.1002/mrm.30115

TECHNICAL NOTE

Magnetic Resonance in Medicine

Fast and High-Resolution T_2 Mapping Based on Echo Merging Plus *k*-t Undersampling with Reduced Refocusing Flip Angles (TEMPURA) as Methods for Human Renal MRI

Hao Li[1,2] | **Andrew N. Priest**[2,3] | **Ines Horvat-Menih**[2] | **Yuan Huang**[2,4] | **Shaohang Li**[1] | **Grant D. Stewart**[5] | **Iosif A. Mendichovszky**[2,3] | **Susan T. Francis**[6] | **Ferdia A. Gallagher**[2,3]

[1]Institute of Science and Technology for Brain-Inspired Intelligence, Fudan University, Shanghai, China
[2]Department of Radiology, University of Cambridge, Cambridge, UK
[3]Department of Radiology, Cambridge University Hospitals NHS Foundation Trust, Addenbrooke's Hospital, Cambridge, UK
[4]EPSRC Cambridge Mathematics of Information in Healthcare Hub, University of Cambridge, Cambridge, UK
[5]Department of Surgery, Cambridge University Hospitals NHS Foundation Trust, Addenbrooke's Hospital, Cambridge, UK
[6]Sir Peter Mansfield Imaging Centre, University of Nottingham, Nottingham, UK

Correspondence
Hao Li, Institute of Science and Technology for Brain-Inspired Intelligence, Fudan University, Shanghai 200433, China.
Email: h_li@fudan.edu.cn

Funding information
Shanghai Municipal Science and Technology Major Project, Grant/Award Number: 2018SHZDZX01; Shanghai Center for Brain Science and Brain-Inspired Technology; The Mark Foundation for Cancer Research, the CRUK Cambridge Centre, Grant/Award Numbers: C9685/A25177, CTRQQR-2021\100012; Shanghai Pujiang Program, Grant/Award Number: 22PJ1400900; National Natural Science Foundation of China, Grant/Award Number: 62201155; Addenbrooke's Charitable Trust, Cambridge University Hospitals; Medical Research Council, Grant/Award Number: MR/R02264X/1; CRUK National Cancer Imaging Translational Accelerator award (NCITA); Cancer Research UK, Grant/Award Numbers: C19212/A27150, C42780/A26854; National Institute for Health and Care Research; Cambridge Experimental Cancer Medicine Centre;

Abstract

Purpose: To develop a highly accelerated multi-echo spin-echo method, TEMPURA, for reducing the acquisition time and/or increasing spatial resolution for kidney T_2 mapping.

Methods: TEMPURA merges several adjacent echoes into one *k*-space by either combining independent echoes or sharing one echo between *k*-spaces. The combined *k*-space is reconstructed based on compressed sensing theory. Reduced flip angles are used for the refocusing pulses, and the extended phase graph algorithm is used to correct the effects of indirect echoes. Two sequences were developed: a fast breath-hold sequence; and a high-resolution sequence. The performance was evaluated prospectively on a phantom, 16 healthy subjects, and two patients with different types of renal tumors.

Results: The fast TEMPURA method reduced the acquisition time from 3–5 min to one breath-hold (18 s). Phantom measurements showed that fast TEMPURA had a mean absolute percentage error (MAPE) of 8.2%, which was comparable to a standardized respiratory-triggered sequence (7.4%), but much lower than a sequence accelerated by purely *k*-t undersampling (21.8%). High-resolution TEMPURA reduced the in-plane voxel size from 3×3 to $1\times1\,mm^2$, resulting in improved visualization of the detailed anatomical structure. In vivo T_2 measurements demonstrated good agreement (fast: MAPE = 1.3%–2.5%; high-resolution: MAPE = 2.8%–3.3%) and high correlation coefficients (fast: $R = 0.85$–0.98; high-resolution: 0.82–0.96) with the standardized method, outperforming *k*-t undersampling alone (MAPE = 3.3–4.5%, $R = 0.57$–0.59).

China 111 Project, Grant/Award Number: B18015; NIHR Cambridge Biomedical Research Centre, Grant/Award Number: NIHR203312; CRUK Cambridge Centre

Conclusion: TEMPURA provides fast and high-resolution renal T_2 measurements. It has the potential to improve clinical throughput and delineate intratumoral heterogeneity and tissue habitats at unprecedented spatial resolution.

KEYWORDS

compressed sensing, imaging acceleration, kidney, multi-echo spin-echo, quantitative MRI, T_2 mapping

1 | INTRODUCTION

MR T_2 relaxation time mapping can provide quantitative T_2 measurements that are independent of confounding factors related to imaging sequences and hardware. This provides a more precise and reproducible method for evaluating the severity of pathological changes compared to conventional T_2-weighted MRI. T_2 values are indicative of tissue composition, particularly free water content, and are sensitive to tissue hydration or edema. In renal imaging, T_2 mapping has shown its potential in evaluating several diseases including autosomal dominant polycystic kidney disease (ADPKD),[1] ischemia–reperfusion injury,[2,3] renal transplants,[4,5] and renal cell carcinoma.[6]

However, routine clinical T_2 mapping has been restricted by the typically long acquisition times, particularly in the abdomen with respiratory triggering. Moreover, the length of time restricts spatial resolution and therefore its ability to probe tissue heterogeneity and tumor habitats, which in turn affects its accuracy in characterizing pathological changes.[7] For instance, the standardized cross-vendor 2D multi-echo spin-echo (MESE) sequence developed for the UK Renal Imaging Network MRI Acquisition and Processing Standardization (UKRIN-MAPS) project[8–10] takes approximately 4 min for a $3 \times 3\,mm^2$ in-plane acquisition, making higher spatial resolution acquisitions impractical for clinical use.

To reduce acquisition times, *k*-space can be undersampled based on parallel imaging and/or compressed sensing (CS) theory.[11–15] Novel pulse sequences, such as MR fingerprinting (MRF),[16] DESPOT2[7] and gradient-spin-echo (GraSE),[17,18] can generate relaxometry maps efficiently, but their accuracy and repeatability may be compromised. For example, studies using MRF revealed higher variation in T_2 measurements compared to their T_1 counterparts,[19,20] and a GraSE-based method demonstrated T_2 overestimation compared to MESE.[17] The time efficiency of MESE as a standard sequence can be improved by combining and filling adjacent echoes into one *k*-space.[21–24] However, the acceleration factor is limited unless combining a large number of echoes, leading to reduction in the number of images available for fitting.

This study introduces a highly accelerated MESE method, termed $\mathbf{T}_2$ mapping using Echo Merging Plus *k*-t Undersampling with Reduced refocusing flip Angles (TEMPURA). A fast breath-hold sequence and a high spatial resolution sequence were both implemented based on TEMPURA. Their performance was compared with the standardized UKRIN-MAPS sequence and a fast sequence accelerated by purely *k*-t undersampling in both phantom and in vivo experiments studying the kidney.

2 | METHODS

2.1 | Acquisition schemes

Figure 1 illustrates the different MESE acquisition schemes investigated in this study. The standardized cross-vendor UKRIN-MAPS sequence is respiratory-triggered and uses a SENSE factor of 3 (Standardized, Figure 1A). To further exploit sparsity, data can be randomly undersampled in both the *ky* and echo dimensions and reconstructed based on the CS theory (*k*-t CS, Figure 1B). The TEMPURA schemes combine every three adjacent echoes into one *k*-space, either by combining three independent echoes (echo-combination, Figure 1C) or sharing one echo between two *k*-spaces (echo-sharing, Figure 1D). The combined *k*-space is still sparsely sampled. Smaller flip angles (175°, 145°, 110° … , 110°) are used for the refocusing pulses to reduce the specific absorption rate (SAR), and thus more echoes can be acquired by using minimum echo spacing.

2.2 | Reconstruction of undersampled *k*-space

For the undersampling reconstruction of *k*-t CS and TEMPURA, we adopted a CS-based method using a self-calibrating temporal principal component analysis (PCA) basis for transform sparsity. Initial images (m_1) were firstly reconstructed from undersampled *k*-space data (k) by the *k*-t FOCUSS approach,[25] which were then used

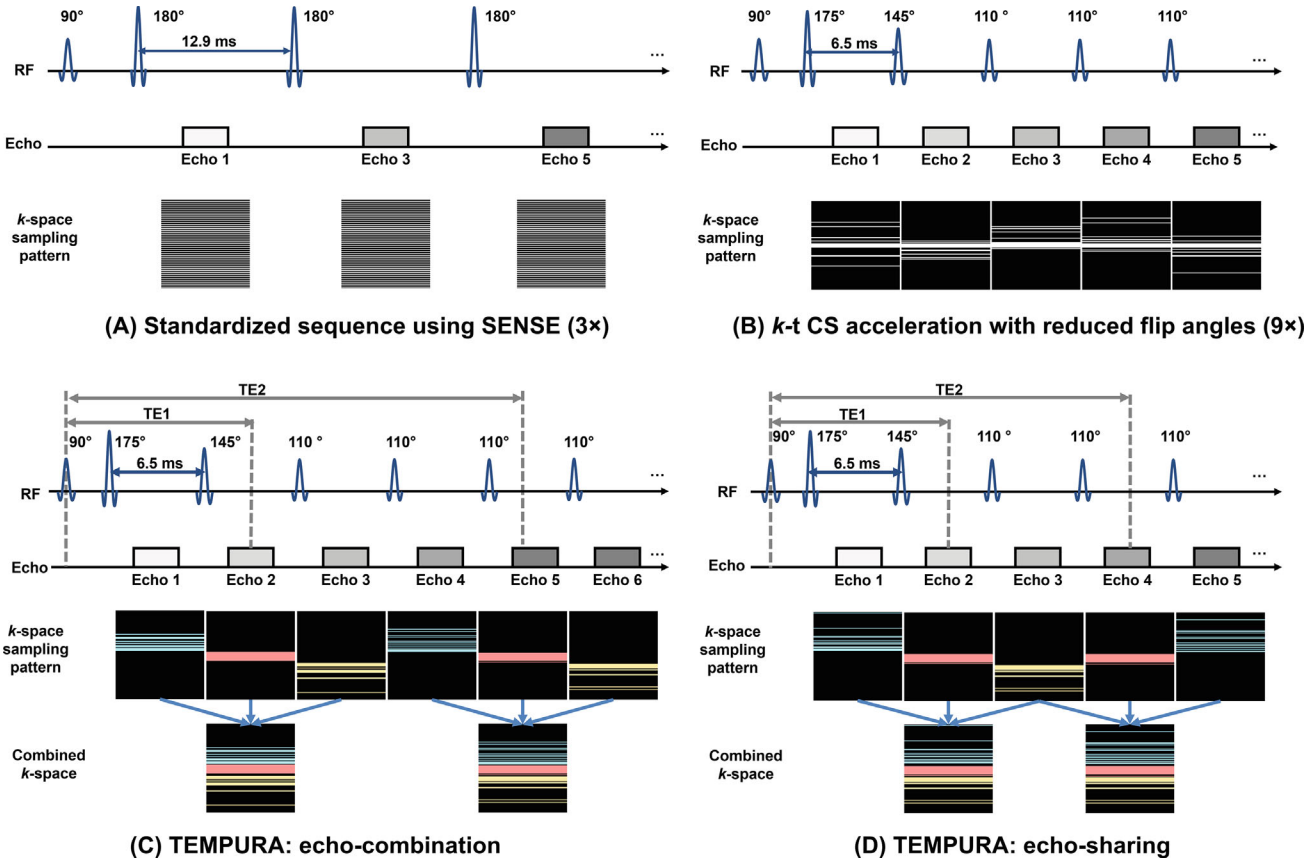

FIGURE 1 Schematic diagram of 2D MESE pulse sequences with different acceleration methods.

to estimate multicoil bases (U) for PCA based on eigen decomposition process[11]:

$$m_1 = kt\text{FOCUSS}(k) = \arg\ \min\ \lambda_1 \left| W^{-1} F_t m \right| + \|Fm - k\|^2 \quad (1)$$

where W is the weight matrix of k-t FOCUSS, and F_t and F are fast Fourier transform along the temporal and spatial dimensions, respectively.

The final images (m_2) were then updated by soft-thresholding using the estimated bases:

$$m_2 = \arg\ \min\ \lambda_2 \left| U^H m \right| + \|\text{FS}m - k\|^2 \quad (2)$$

where coil sensitivity (S) was estimated from a compact calibration region of k-space data using the ESPIRiT method.[26] The regularization parameters λ_1 and λ_2 were optimized and both set to 0.001 in the study.

2.3 | Fitting using the extended phase graph model

To address the indirect echoes resulting from reduced refocusing flip angles, we use an extended phase graph (EPG) model,[27] adapted from the StimFit toolbox,[28,29] for fitting in this study:

$$(T_2, M_0) = \text{argmin} \sum_{i=1}^{\text{ETL}} \|M_0 \cdot \text{EPG}(T_1, T_2, FA, B_1, \text{ESP}) - S_i\| \quad (3)$$

where T_2 can be calculated based on the known values of T_1, refocusing flip angle (FA), echo spacing (ESP), echo train length (ETL), and signal intensity of each echo S_i. Considering that the EPG model is not sensitive to T_1 variation,[28] a fixed T_1 of 1500 ms was used in all processing. For TEMPURA, a fixed refocusing FA of 110° without scaling of transmit field B_1 was used due to challenges in fitting B_1 variation within the echo merging scheme.

2.4 | Imaging protocol and implementation

Two versions of the TEMPURA sequence were developed: one highly accelerated single breath-hold sequence and one high-resolution respiratory-triggered sequence using a larger matrix size. Parameters for each of the sequences are shown in Table 1.

All experiments were performed on a 3T scanner (Discovery MR750; GE Healthcare, Waukesha, WI) with a

TABLE 1 Key parameters of the different MESE-based T_2 mapping sequences.

Method	Acceleration	TE (min:Δ:max)	TR (ms)	FA	Resolution (mm)	Bandwidth (Hz/pixel)	Acq. time (min:s)
Reference							
NIST	None	10:10:320 (32 echoes)	5000	180°	1 × 1.3	227	16:10 (1 slice)
UKRIN Standardized	SENSE: 3×	12.9:12.9:129 (10 echoes)	1 breath (phantom, 3750)	180°	3 × 3	244	43 breaths (phantom, 2:49)
Breath-hold							
k-t CS	Undersamp.: 9.4×	6.5:6.5:195 (30 echoes)	1125	110°	3 × 3	976	0:18
TEMPURA: echo-comb.	Echo-comb: 3 × Undersampling: 3.1×	13:19.5:188.5 (30 echoes, merged into 10)	1125	110°	3 × 3	976	0:18
TEMPURA: echo-sharing	Echo-sharing: 3 × Undersampling: 3.1×	13:13:195 (30 echoes, merged into 15)	1125	110°	3 × 3	976	0:18
High-resolution							
TEMPURA	Echo-sharing: 3 × Undersampling: 3.1×	15.6:15.6:234 (30 echoes, merged into 15)	1 breath (phantom, 3750)	110°	1 × 1	326	43 breaths (phantom, 2:49)

Note: Other parameters in common: FOV = 384 mm, five slices with thickness/gap of 4.5/1.0 mm (except NIST: FOV = 250 mm, one slice with thickness 6 mm).

32-channel cardiac array coil. Sequence and reconstruction parameters were optimized based on measurements from the ISMRM/NIST phantom.[30] Original T_2-weighted images were reconstructed from undersampled data after echo emerging in *k*-space, then fitted using the EPG model based on the StimFit toolbox.[28,29] All processing was performed offline using MATLAB (MathWorks, Natick MA). The average computation times were 2.2 and 7.8 min for breath-holding and high-resolution acquisitions (Intel i9-13900KF, 64 GB RAM).

2.5 | Phantom experiments

The ISMRM/NIST system phantom[30] was used to evaluate the accuracy of T_2 measurements against temperature-corrected reference values.[31] The plate containing 13 T_2 spheres filled with $MnCl_2$-doped water and a resolution inset was scanned using previously described sequences, together with the single-slice fully sampled NIST reference sequence (see Table 1).

Two studies were conducted to assess the impact of TEMPURA on (1) acceleration and (2) spatial resolution. The acceleration evaluation involved acquisitions with a fixed matrix size (128 × 128) but varying the acceleration factor (×1, ×3.3, ×6.5, ×9.4, and ×11.3), corresponding to acquisition times of 2:40, 0:51, 0:26, 0:18 and 0:15 (min:s). The TR was reduced to 1125 ms to further reduce the acquisition time. For the spatial resolution evaluation, sequences had a fixed acquisition time (2:49, matched to the standardized UKRIN acquisition) but were collected at seven different matrix sizes (128 × 128, 192 × 192, 256 × 256, 320 × 320, 384 × 384, 448 × 448, and 512 × 512), resulting in in-plane spatial resolutions from 3.00 to 0.75 mm. Each sequence was repeated three times.

2.6 | In vivo experiments

The kidneys of 16 healthy subjects (9 men; 7 women; range 24–47 y), one patient with a renal oncocytoma (male, 74 y), and one patient with clear cell renal cell carcinoma (ccRCC) (male, 62 y) were prospectively imaged. Studies were approved by the local research ethics committee, and all participants gave informed consent.

The standardized UKRIN sequence, breath-hold TEMPURA sequence with echo-sharing, *k*-t CS, and the high-resolution TEMPURA sequence with echo-sharing (384 × 384) were collected on each subject. Synthetic T_2-weighted images were generated from the high-resolution T_2 and M_0 maps without additional acquisitions. A separate T_2-weighted 3D fast spin echo (FSE) sequence was also collected on the patient (respiratory-triggered, FOV 400 × 360 × 192 mm, matrix 256 × 224 × 48, TE/TR 67.9/8574 ms, echo train length 120).

Regions of interest (ROIs) were manually drawn on the standardized UKRIN T_2 maps to define the whole kidney,

and renal cortex and medulla. Minor manual adjustments were made to correct for motion to apply these ROIs to the T_2 maps generated for the other sequences. The mean T_2 values from the cortex, medulla and whole kidney were measured.

2.7 | Statistical analysis

In phantom experiments, accuracy of T_2 measurements was assessed by calculating mean absolute percentage error (MAPE) and pixelwise RMS error (RMSE) against reference values (T_2^{ref}) for seven spheres within the physiologically relevant range (42–405 ms).

MAPE assesses the overall bias between the averaged T_2 values of each sphere and the reference values:

$$\mathrm{MAPE} = \frac{100\%}{N_{\mathrm{sphere}}} \sum_{i=1}^{N_{\mathrm{sphere}}} \frac{\left|\mathrm{mean}(\mathbf{T_{2}}_{i}) - \mathrm{T}_{2\ i}^{\mathrm{ref}}\right|}{\mathrm{T}_{2\ i}^{\mathrm{ref}}} \tag{4}$$

RMSE compares all pixels in selected spheres with the reference values on a pixel-by-pixel basis:

$$\mathrm{RMSE}_{\mathrm{pixel}} = \sqrt{\frac{1}{N_{\mathrm{pixel}}} \sum_{i=1}^{N_{\mathrm{pixel}}} \left(\mathbf{T_2} - \mathrm{T}_2^{\mathrm{ref}}\right)^2} \tag{5}$$

SNR was measured to evaluate the image quality of the original T_2-weighted images. The noise level was estimated by placing an ROI on deionized water filling, which has a long T_2, and calculating the standard deviation of signals across both the ROI and echoes. The signal level was estimated by averaging the signal intensity across the entire phantom.

For phantom experiments, all repeated measurements were compared with the phantom reference values using a random-intercept linear mixed-effects model (details in Appendix A). For in vivo experiments, the results of all methods were compared with the reference measurements obtained by the standardized UKRIN method using MAPE, a paired Student's *t*-test, Pearson correlation analysis and Bland–Altman analysis. *P* values <0.05 were considered to be statistically significant in all analyses.

3 | RESULTS

The results of the T_2 measurement in the ISMRM/NIST system phantom are presented in Figure 2. Figure 2A,B show the MAPE, $\mathrm{RMSE}_{\mathrm{pixel}}$, and SNR for the different acceleration factors to collect images at a given 3 mm in-plane spatial resolution, and for different matrix sizes in a given acquisition time, respectively. Figure 2C shows the regression plots of the T_2 measurements in each sphere against reference values across selected acquisitions. Among the three acceleration methods, TEMPURA with echo-sharing demonstrates the highest accuracy. Compared to the standardized method, the acquisition time can be reduced from 169 to 18 s, with the MAPE of TEMPURA (8.2% at 9.4×) remaining comparable to the standardized UKRIN method (7.4%) but much lower than that of *k*-t CS (21.8% at 9.4×). TEMPURA also outperformed *k*-t CS in $\mathrm{RMSE}_{\mathrm{pixel}}$ (TEMPURA 9.4×: 19.9, *k*-t CS 9.4×: 36.9, standardized: 12.9) and SNR (TEMPURA 9.4×: 13.5, *k*-t CS 9.4×: 11.9, standardized: 16.1).

Employing larger matrix sizes to increase the spatial resolution in TEMPURA echo-sharing greatly improved the visualization of the detailed structure without increasing the acquisition time. High-resolution TEMPURA exhibits reduced MAPE values (4.8% and 6.1% for 384×384 and 512×512) compared to the standardized method, possibly due to a larger number of samples and less partial volume effect resulting from increased resolution. The $\mathrm{RMSE}_{\mathrm{pixel}}$ and SNR of high-resolution TEMPURA are similar to the standardized method.

Significant differences between T_2 measurements and reference values were only found in *k*-t CS at 9.4× ($p = 0.001$) and 11.3× ($p < 0.001$), TEMPURA echo-sharing at 11.3× ($p = 0.02$), and TEMPURA echo-combination at 11.3× ($p < 0.001$) (Table S1).

Figure 3 shows representative results from a healthy volunteer, a patient with an oncocytoma, and a patient with a ccRCC. In Figure 3A, single breath-hold TEMPURA produced comparable image quality to the standardized UKRIN MESE sequence, whereas *k*-t CS led to image blurring. High-resolution TEMPURA with a 3× matrix size substantially enhanced the imaged anatomical detail in the kidney, allowing the cortex and medulla to be distinguished on the T_2 map. In Figure 3B,C, while breath-hold TEMPRUA yields T_2 maps similar to standard MESE, high-resolution TEMPURA improves the tumor visualization in patient images, enabling clear observation of its detailed structure and T_2 distribution of the habitats within the tumor. The synthetic T_2-weighted image shows superior image quality and anatomical detail compared to the T_2-weighted images acquired by a separate 3D FSE sequence.

In vivo T_2 measurements from the volunteers are shown in Table 2 and Bland–Altman plots in Figure S1. Using the standardized UKRIN method as the reference, both breath-hold and high-resolution TEMPURA echo-sharing achieved good agreement (MAPE = 1.31%–2.50% and 2.80%–3.28%, respectively) and high correlation coefficient ($R = 0.85$–0.98 and 0.82–0.96, respectively; $p < 0.001$), whereas *k*-t CS showed a much lower correlation (0.57–0.59, $p < 0.05$) and higher

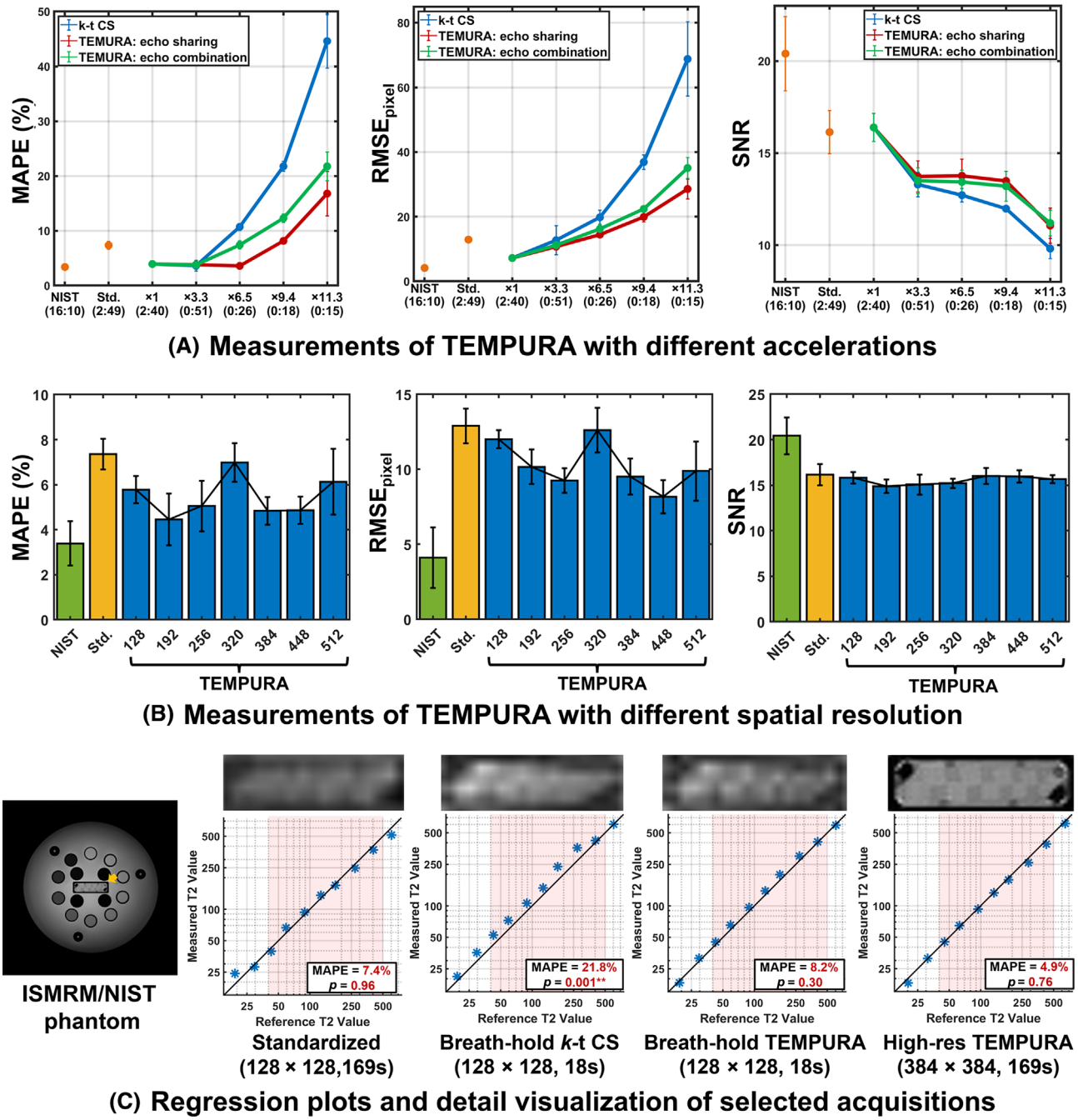

FIGURE 2 Quantitative evaluation of T_2 measurements from the NIST phantom. (A) MAPE, $RMSE_{pixel}$, and SNR of T_2 measurements using different acceleration methods with different acquisition times. The matrix size is 128 × 128 for all acquisitions. (B) MAPE, $RMSE_{pixel}$, and SNR of T_2 measurements using TEMPURA (echo-sharing) with different matrix sizes. The acquisition time is 169 s for all TEMPURA acquisitions and the standardized acquisition. (C) Regression plots indicating measurements from T_2 spheres in comparison with the NIST reference values. Red rectangular boxes indicate physiologically meaningful ranges (45–500 ms). Upper images show the resolution inset (indicated by the yellow arrow on the phantom image) cropped from corresponding source images (TE = ~40 ms).

MAPE (3.28%–4.45%). No significant difference was found between each method and the standardized method except the T_2 measurements in medulla for *k*-t CS and high-resolution TEMPURA.

The signal evolution and fitting curves of TEMPURA and standard MESE are displayed in Figure S2. TEMPURA exhibited a slower signal decay due to using smaller refocusing FAs, yet both methods yielded similar T_2 measurements. The standard MESE shows zigzag curves caused by B_1 inhomogeneity, whereas TEMPURA with echo-sharing fills even echoes into the inner portion of *k*-space and results in smoother signal evolution curves.

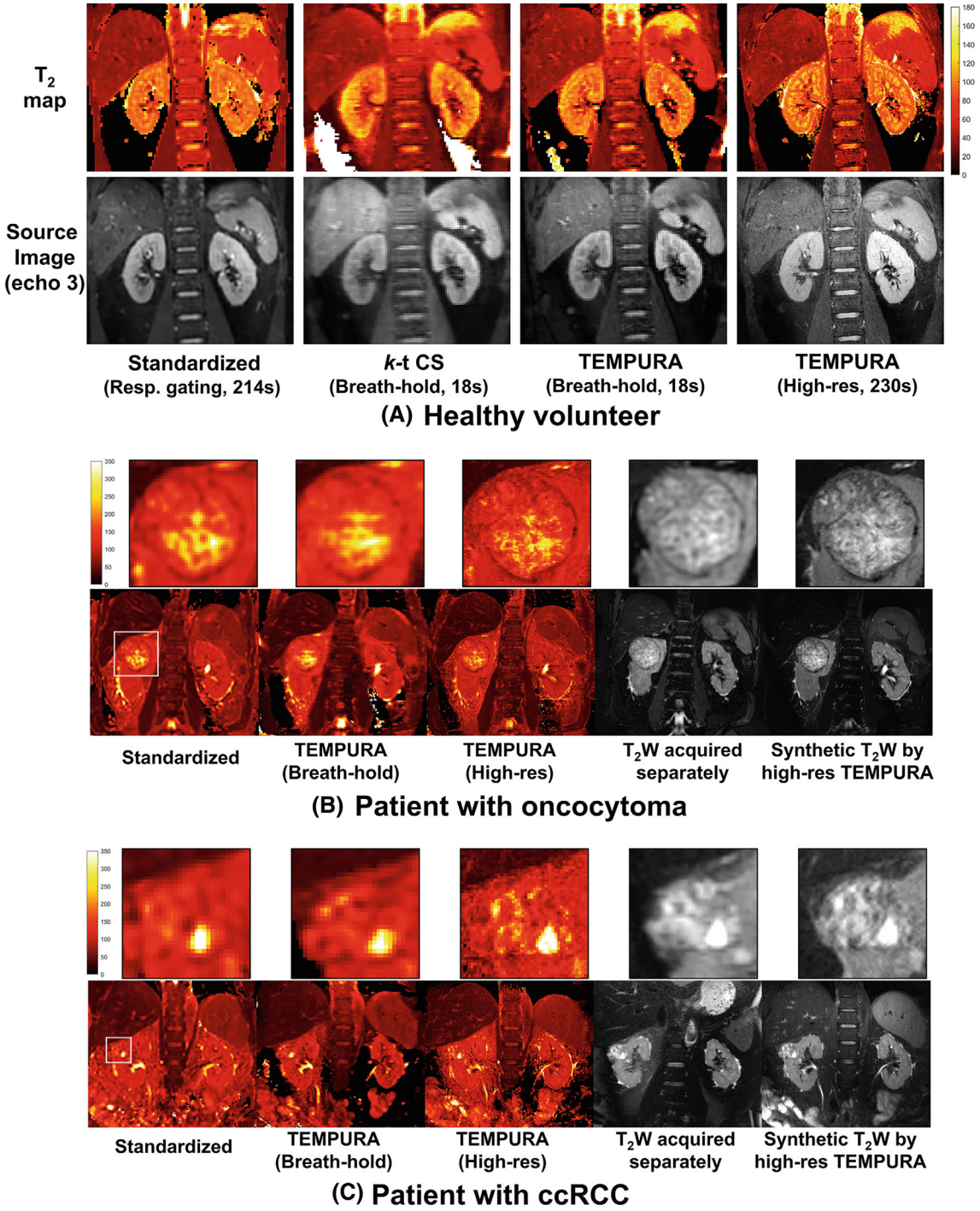

FIGURE 3 Representative images from a healthy volunteer (A), a patient (male, 73 y) diagnosed with an oncocytoma (B) and a patient (male, 62 y) diagnosed with ccRCC (C). In (A), breath-hold TEMPURA produced similar image quality as the standardized method, while *k*-t CS resulted in blurred images. High-resolution TEMPURA enhanced the anatomical detail, allowing differentiation between the cortex and medulla. In (B) and (C), high-resolution TEMPURA enabled clear observation of its detailed structure and T_2 distribution. The upper row shows zoomed-in views of the tumor region. The synthetic T_2-weighted image (TE = 162 ms) also shows greater anatomical detail compared to the T_2-weighted images acquired by a separate 3D FSE sequence.

4 | DISCUSSION

We have presented TEMPURA, a highly accelerated and high spatial resolution method for T_2 mapping based on *k*-t undersampling and echo merging. Reduced refocusing FAs allowed for more echoes within SAR limits. TEMPURA outperformed the *k*-t CS method that simply undersamples *k*-space, maintaining low errors and no significant difference from the reference T_2 values when the acceleration factor was no greater than 9.4×. The high

TABLE 2 Comparison of T_2 measurements from 16 healthy volunteers using TEMPURA and *k*-t CS versus the standardized method.

Parameter	Whole kidney	Cortex	Medulla
UKRIN standardized			
T_2	104.0 ± 5.2	99.2 ± 5.0	109.3 ± 6.6
Beath-hold *k*-t CS			
T_2	103.1 ± 4.1	99.1 ± 5.0	106.0 ± 5.1*
MAPE	3.28%	3.99%	4.45%
Pearson *R (P)*	0.59 (0.03)	0.57 (0.02)	0.59 (0.02)
Breath-hold TEMPURA			
T_2	103.9 ± 5.7	100 ± 5.1	108.3 ± 7.4
MAPE	1.91%	2.50%	1.31%
Pearson *R (P)*	0.90 (<0.001)	0.85 (<0.001)	0.98 (<0.001)
High-res TEMPURA			
T_2	105.1 ± 6.9	100.7 ± 6.3	112.5 ± 9.2*
MAPE	2.80%	3.17%	3.28%
Pearson *R (P)*	0.92 (<0.001)	0.82 (<0.001)	0.96 (<0.001)

Note: MAPE, Pearson correlation coefficients, and paired Student's *t*-tests are calculated between each method and the standardized method.
*Denotes statistical significance ($P < 0.05$).

time efficiency enables a fast breath-holding acquisition, greatly reducing the acquisition time of renal T_2 mapping from approximately 4 min to a single breath-hold of 18 s.

Moreover, the acceleration of TEMPURA was utilized to increase the spatial resolution without prolonging the acquisition time, enhancing visualization of detailed anatomy within the kidney and facilitating the improved differentiation of renal cortex and medulla. The improved resolution also allowed the identification of intratumoral heterogeneity and tissue habitats within a renal mass, which could benefit tumor stratification and texture analysis. Synthetic T_2-weighted images across variable TEs were generated without additional acquisitions: compared with the 3D FSE sequence, synthetic T_2-weighted images provided a clearer depiction of the renal anatomy and the intratumoral heterogeneity due to the higher resolution and less T_2 blurring caused by mixing *k*-space data from different echoes.[23] This high-resolution T_2 mapping approach, along with the synthetic T_2-weighted images, may be used for investigating disease-related changes in both morphology and quantitative T_2 values.

In this study, we demonstrated that echo-sharing is more accurate than echo-combination for merging echoes in TEMPURA, possibly due to two factors. First, echo-sharing allocates all even echoes into the inner portion of *k*-space, and even echoes are more accurate than odd echoes for T_2 quantification in MESE.[32] Second, the echo sharing approach allows for smaller ΔTE and more echoes, which is advantageous when measuring small T_2 components.

While we set the number of combined echoes to three in this study, it may be further increased for acquisitions involving more echoes. Multi-compartment T_2 acquisitions based on MESE are particularly suitable for TEMUPRA due to their long TEs and large echo numbers. This allows for combining more echoes and using higher *k*-t undersampling factors. Future studies will investigate the application of TEMPURA in multi-compartment T_2 acquisitions, such as luminal water imaging in the prostate.[33]

TEMPURA achieves a 9.4-fold acceleration, surpassing previous *k*-t CS models (2- to 3-fold in (12) and 4- to 8-folds in (13)) and deep-learning methods using purely undersampling (8-fold in (14) and (15)). While GraSE presents as another rapid sequence,[17,18] its utilization of gradient echoes with lower SNR and T_2* weighting may cause T_2 overestimation,[18] image blurring,[34] as well as peripheral nerve stimulation and acoustic noise.[34] TEMPURA merges spin echoes with small echo spacings, potentially alleviating these issues. MARTINI[22] and GRAPPATINI[23] also merge adjacent echoes of MESE but lack CS reconstruction or reduced FAs. While MATINI/-GRAPPATINI showed a 10-fold acceleration, they were only used for acquisitions with large matrix sizes (260 × 320–512 × 270) and long acquisition times (2:50–6:22), unlike TEMPURA's more challenging single breath-hold acquisitions. Future studies should comprehensively compare TEMPURA with other methods.

This study has several limitations. First, the current fitting method is a simplified EPG-based model that does not fully consider the echo merging scheme and B_1 inhomogeneity, which will be improved in future work. Second, manual placing ROIs on standardized T_2 maps for the cortex and medulla might compromise accuracy due to the difficulty in distinguishing these regions on low-resolution T_2 maps. Furthermore, image misregistration between T_2 maps acquired by different methods may not be fully corrected by manual adjustment in this study, particularly between breath-hold and respiratory triggered methods. With a more robust image registration method, signal heterogeneity analysis and comparison can also be performed. Third, a repeatability evaluation comparing the in vivo scan-rescan variability of TEMPURA with other methods should be performed in future work. Fourth, to address potential challenges associated with offline processing in clinical implementation, efforts should focus on developing faster online

reconstruction and fitting methods using high-speed programming languages. Last, we have only demonstrated this method for renal T_2 mapping, and only two patients were imaged as part of this study. TEMUPRA has potential to be applied in various other anatomical regions. The breath-hold version could be particularly beneficial for other organs that experience respiratory motion, such as the liver, spleen, pancreas and cardiac measurement. Future research will investigate the performance of TEMPURA in larger cohorts of patients and across other body regions.

5 | CONCLUSIONS

We have developed single breath-hold and high spatial resolution renal T_2 mapping sequences using a new acceleration method termed TEMPURA. The breath-hold sequence offers a rapid and accurate T_2 measurement, which can be potentially used for the diagnosis of renal diseases requiring quick examinations. The high-resolution sequence provides the distinct depiction of anatomical structures within the kidney, facilitating in depth evaluation of both anatomical morphology and quantitative T_2 values for a diverse range of pathological conditions including intratumoral heterogeneity.

ACKNOWLEDGMENTS

This work was supported by Cancer Research UK (CRUK; C19212/A27150; C42780/A26854), the CRUK Cambridge Centre, The National Institute for Health and Care Research (NIHR) Cambridge Biomedical Research Centre, Cambridge Experimental Cancer Medicine Centre, CRUK National Cancer Imaging Translational Accelerator award (NCITA), Addenbrooke's Charitable Trust, and the UKRIN-MAPS Medical Research Council Grant (MR/R02264X/1). Hao Li is supported by National Natural Science Foundation of China (No. 62201155), the Shanghai Pujiang Program (No. 22PJ1400900), Shanghai Municipal Science and Technology Major Project (No. 2018SHZDZX01), ZJ Lab, Shanghai Center for Brain Science and Brain-Inspired Technology, and the China 111 Project (No. B18015). Grant D Stewart is supported by The Mark Foundation for Cancer Research, the CRUK Cambridge Centre (C9685/A25177 and CTRQQR-2021\100012) and NIHR Cambridge Biomedical Research Centre (NIHR203312). The views expressed are those of the author(s) and not necessarily those of the NIHR or the Department of Health and Social Care.

DATA AVAILABILITY STATEMENT

The reconstruction and fitting code, along with example datasets supporting the study findings, will be publicly accessible on GitHub at https://github.com/hl476-cam/TEMPURA.

ORCID

Hao Li https://orcid.org/0000-0002-7712-0890

Andrew N. Priest https://orcid.org/0000-0002-9771-4290

REFERENCES

1. Franke M, Baeßler B, Vechtel J, et al. Magnetic resonance T_2 mapping and diffusion-weighted imaging for early detection of cystogenesis and response to therapy in a mouse model of polycystic kidney disease. *Kidney Int*. 2017;92:1544-1554. doi:10.1016/j.kint.2017.05.024
2. Hueper K, Rong S, Gutberlet M, et al. T_2 relaxation time and apparent diffusion coefficient for noninvasive assessment of renal pathology after acute kidney injury in mice: comparison with histopathology. *Invest Radiol*. 2013;48:834-842. doi:10.1097/RLI.0B013E31829D0414
3. Chen J, Chen Q, Zhang J, et al. Value of T_2 mapping in the dynamic evaluation of renal ischemia-reperfusion injury. *Acad Radiol*. 2022;29:376-381. doi:10.1016/J.ACRA.2021.03.004
4. Mathys C, Blondin D, Wittsack HJ, et al. T_2' imaging of native kidneys and renal allografts - a feasibility study. RoFo Fortschritte auf dem Gebiet der Rontgenstrahlen und der Bildgeb. *Verfahren*. 2011;183:112-119. doi:10.1055/s-0029-1245597
5. Adams LC, Bressem KK, Scheibl S, et al. Multiparametric assessment of changes in renal tissue after kidney transplantation with quantitative MR relaxometry and diffusion-tensor imaging at 3 T. *J Clin Med*. 2020;9:1-16. doi:10.3390/jcm9051551
6. Adams LC, Bressem KK, Jurmeister P, et al. Use of quantitative T_2 mapping for the assessment of renal cell carcinomas: first results. *Cancer Imaging*. 2019;19:1-11. doi:10.1186/s40644-019-0222-8
7. Deoni SCL, Peters TM, Rutt BK. High-resolution T_1 and T_2 mapping of the brain in a clinically acceptable time with DESPOT1 and DESPOT2. *Magn Reson Med*. 2005;53:237-241. doi:10.1002/mrm.20314
8. Li H, Buchanan CE, Morris DM, et al. Improved harmonization of renal T_2 mapping between vendors using stimulated echo compensation. In: Proceedings of Joint Annual Meeting ISMRM-ESMRMB & ISMRT 31st Annual Meeting; 2022. p. 4409.
9. Buchanan CE, Li H, Morris DM, et al. A travelling kidney study using a harmonised multiparametric renal MRI protocol. In: Proceedings of the 27th Annual Meeting of ISMRM, Montreal, Canada; 2022. p. 482.
10. Li H, Daniel AJ, Buchanan CE, et al. Improvements in between-vendor MRI harmonization of renal T_2 mapping using stimulated echo compensation. *J Magn Reson Imaging*. 2024. doi:10.1002/jmri.29282
11. Feng L, Otazo R, Jung H, et al. Accelerated cardiac T_2 mapping using breath-hold multiecho fast spin-echo pulse sequence with k-t FOCUSS. *Magn Reson Med*. 2011;65:1661-1669. doi:10.1002/mrm.22756
12. Zhang T, Pauly JM, Levesque IR. Accelerating parameter mapping with a locally low rank constraint. *Magn Reson Med*. 2015;73:655-661. doi:10.1002/mrm.25161

13. Peng X, Ying L, Liu Y, Yuan J, Liu X, Liang D. Accelerated exponential parameterization of T_2 relaxation with model-driven low rank and sparsity priors (MORASA). *Magn Reson Med*. 2016;76:1865-1878. doi:10.1002/mrm.26083
14. Liu F, Feng L, Kijowski R. MANTIS: model-augmented neural network with incoherent k-space sampling for efficient MR parameter mapping. *Magn Reson Med*. 2019;82:174-188. doi:10.1002/mrm.27707
15. Meng Z, Guo R, Li Y, et al. Accelerating T_2 mapping of the brain by integrating deep learning priors with low-rank and sparse modeling. *Magn Reson Med*. 2021;85:1455-1467. doi:10.1002/mrm.28526
16. Ma D, Gulani V, Seiberlich N, et al. Magnetic resonance fingerprinting. *Nature*. 2013;495:187-192. doi:10.1038/nature11971
17. Baeßler B, Schaarschmidt F, Stehning C, Schnackenburg B, Maintz D, Bunck AC. Cardiac T_2-mapping using a fast gradient echo spin echo sequence - first in vitro and in vivo experience. *J Cardiovasc Magn Reson*. 2015;17:17. doi:10.1186/s12968-015-0177-2
18. Sprinkart AM, Luetkens JA, Träber F, et al. Gradient spin Echo (GraSE) imaging for fast myocardial T_2 mapping. *J Cardiovasc Magn Reson*. 2015;17:1-9. doi:10.1186/s12968-015-0127-z
19. Körzdörfer G, Kirsch R, Liu K, et al. Reproducibility and repeatability of MR fingerprinting relaxometry in the human brain. *Radiology*. 2019;292:429-437. doi:10.1148/radiol.2019182360
20. Buonincontri G, Biagi L, Retico A, et al. Multi-site repeatability and reproducibility of MR fingerprinting of the healthy brain at 1.5 and 3.0 T. *Neuroimage*. 2019;195:362-372. doi:10.1016/J.NEUROIMAGE.2019.03.047
21. Kim D, Jensen JH, Wu EX, Sheth SS, Brittenham GM. Breathhold multiecho fast spin-echo pulse sequence for accurate R^2 measurement in the heart and liver. *Magn Reson Med*. 2009;62:300-306. doi:10.1002/mrm.22047
22. Sumpf TJ, Uecker M, Boretius S, Frahm J. Model-based nonlinear inverse reconstruction for T_2 mapping using highly undersampled spin-echo MRI. *J Magn Reson Imaging*. 2011;34:420-428. doi:10.1002/jmri.22634
23. Hilbert T, Sumpf TJ, Weiland E, et al. Accelerated T_2 mapping combining parallel MRI and model-based reconstruction: GRAPPATINI. *J Magn Reson Imaging*. 2018;48:359-368. doi:10.1002/jmri.25972
24. Mekle R, Laine AF, Wu EX. Combined MR data acquisition of multicontrast images using variable acquisition parameters and K -space data sharing. *Combined MR Data Acquisition of Multicontrast*. 2003;22:806-823.
25. Jung H, Sung K, Nayak KS, Kim EY, Ye JC. k-t FOCUSS: a general compressed sensing framework for high resolution dynamic MRI. *Magn Reson Med*. 2009;61:103-116. doi:10.1002/mrm.21757
26. Uecker M, Lai P, Murphy MJ, et al. ESPIRiT - an eigenvalue approach to autocalibrating parallel MRI: where SENSE meets GRAPPA. *Magn Reson Med*. 2014;71:990-1001. doi:10.1002/mrm.24751
27. Hennig J. Multiecho imaging sequences with low refocusing flip angles. *J Magn Reson*. 1988;78:397-407. doi:10.1016/0022-2364(88)90128-X
28. Lebel RM, Wilman AH. Transverse relaxometry with stimulated echo compensation. *Magn Reson Med*. 2010;64:1005-1014. doi:10.1002/mrm.22487
29. Lebel RM. StimFit: a toolbox for robust T_2 mapping with stimulated echo compensation. In: Proceedings from the 20th Annual Meeting of ISMRM, Melbourne, Australia. Vol. 37; 2012. p. 2558.
30. Stupic KF, Ainslie M, Boss MA, et al. A standard system phantom for magnetic resonance imaging. *Magn Reson Med*. 2021;86:1194-1211. doi:10.1002/mrm.28779
31. Statton BK, Smith J, Finnegan ME, Koerzdoerfer G, Quest RA, Grech-Sollars M. Temperature dependence, accuracy, and repeatability of T_1 and T_2 relaxation times for the ISMRM/NIST system phantom measured using MR fingerprinting. *Magn Reson Med*. 2021;87:1446-1460. doi:10.1002/MRM.29065
32. Kucharczyk W, Brant-Zawadzki M, Lemme-Plaghos L, et al. MR technology: effect of even-echo rephasing on calculated T_2 values and T_2 images. *Radiology*. 1985;157:95-101. doi:10.1148/radiology.157.1.4034984
33. Sabouri S, Chang SD, Savdie R, et al. Luminal water imaging: a new MR imaging T_2 mapping technique for prostate cancer diagnosis. *Radiology*. 2017;284:451-459. doi:10.1148/radiol.2017161687
34. Dvorak AV, Wiggermann V, Gilbert G, et al. Multi-spin echo T_2 relaxation imaging with compressed sensing (METRICS) for rapid myelin water imaging. *Magn Reson Med*. 2020;84:1264-1279. doi:10.1002/mrm.28199

SUPPORTING INFORMATION

Additional supporting information may be found in the online version of the article at the publisher's website.

Figure S1. Bland–Altman plots comparing the T_2 measurements in the whole kidney, renal cortex and medulla between three accelerated methods and the standardized method. The difference is defined as $T_{2\text{accelerated}} - T_{2\text{standardized}}$.

Figure S2. Signal evolution curves and fitting curves of TEMPURA (echo-sharing) and the standardized MESE method. (A) Signal from the NIST/ISMRM phantom (reference $T_2 = 89.1$ ms) (B) Signal from the renal cortex of a healthy volunteer. The slower signal decay of TEMPURA is attributed to its use of smaller refocusing flip angles (110°).

Table S1. T_2 measurements from the ISMRM/NIST phantom.

How to cite this article: Li H, Priest AN, Horvat-Menih I, et al. Fast and High-Resolution T_2 Mapping Based on Echo Merging Plus *k*-t Undersampling with Reduced Refocusing Flip Angles (TEMPURA) as Methods for Human Renal MRI. *Magn Reson Med*. 2024;92:1138-1148. doi: 10.1002/mrm.30115

APPENDIX A

A.1 STATISTICAL ANALYSIS FOR PHANTOM EXPERIMENTS

In the phantom experiment, T_2 spheres were scanned using different sequences, with each sequence repeated three times. Such repeated measures allowed more precise assessment of sequence performance, but also created a data hierarchy as observations were no longer independent. This would violate the basic assumption of conventional statistical approaches.

We used a random-intercept linear mixed-effects (LME) model to address this issue. Data were entered as proportions to the ground-truth T_2 values. A categorical variable describing the acquisition method was studied as the fixed effect, and the intercept for specimen was modeled as the random effect. The p values of the fixed effect were calculated using the Satterthwaite's degrees of freedom method. The analysis was performed in R 4.2.2 with packages 'lme4' and 'lmerTest'.